Molecular Dynamics Simulations of Oxygen Transport through a Fully Atomistic Polyimide Membrane

Sylvie Neyertz* and David Brown

LMOPS-UMR CNRS 5041, University of Savoie, Bât IUT, 73376 Le Bourget du Lac Cedex, France

Received November 30, 2007; Revised Manuscript Received January 24, 2008

ABSTRACT: Oxygen (O_2) transport through a fully atomistic glassy ODPA−ODA polyimide free-standing membrane has been studied using large-scale molecular dynamics (MD) simulations. Both the polymer matrix and the penetrants were described with a realistic force field, including full excluded-volume and electrostatic interactions, and the total number of atoms amounted to 65 480. The polyimide had the typical features of surface layers, i.e., flattened chain configurations which led to a density corresponding to ∼97% of the bulk density, surface roughness, and increased mobility at the interface. Oxygen penetration and diffusion through this membrane model was followed over a total of 13 000 ps. Bulk models were also studied for comparison. In the membrane, O_2 exhibits two distinct mobility modes. The first one is associated with the adsorption of the gas at the polymer interface, which is driven by the strong solubility gradient in this region and where the mobility remains fairly close to that in the gas phase. The second one is a much slower and limiting diffusion mode with a boundary situated at the start of the denser part of the matrix. The diffusion here was found to be anomalous at short time intervals in a similar way to that in the bulk. It eventually became Fickian at longer time intervals irrespective of the definition of the membrane width and showed that it is mostly governed by the density of the matrix. Such polymer interfacial structures are thus associated with an increase in both solubility and diffusion.

1. Introduction

Glassy polyimides are of great interest as dense membranes for gas separation, since they combine excellent mechanical, thermal, and chemical stabilities with a large range of penetrant selectivities. Their permeabilities with respect to e.g. oxygen, nitrogen, carbon dioxide, or methane are partially governed by the chain chemical structures, which can be derived from a large variety of aromatic or alicyclic dianhydride and diamine motives.[1–4] Following polymer synthesis, the membranes are usually prepared by dissolving the polymer in a solvent (such as *m*-cresol or *N*-methylpyrrolidone), casting the solution on a substrate, and completing with an appropriate thermal treatment.[5] It is well-known that each step of the processing procedure is also likely to affect the film permeation properties.[6–8] This is the case for e.g. the solvent used,[9,10] the casting surfaces and conditions,[11] the heating cycle,[11,12] or the sample thicknesses.[13,14] Polyimide membranes can be quite sensitive to physical aging as well.[15–17]

Molecular dynamics (MD) simulations[18] are now widely used to characterize both the underlying structures and dynamics at the molecular level, providing that appropriate models can be built. It is comparatively a lot easier and computationally less expensive to build and run polyimide + gas bulk simulations,[19–29] rather than real membrane models with explicit surfaces. However, bulk models cannot possibly reveal any "skin effects". We have thus recently designed a procedure loosely based on the experimental solvent-casting process for creating a fully atomistic 40-mers ODPA−ODA polyimide (Figure 1) membrane model.[28,30,31] Since the radius of gyration of the polymer $\langle S^2 \rangle^{1/2}$ is usually quoted as being the minimum distance for the influence of an interface,[32–39] the target width of our initial model was set to $2\langle S^2 \rangle^{1/2}$, i.e., a total of 141 100 atoms in 68 ODPA−ODA chains. This led to a membrane of width ∼130 Å confined by a wall[30] and, upon removal of the wall constraint, to a free-standing membrane of width ∼140 Å.[31] While such dimensions remain relatively small with respect to experimental thicknesses of a few microns,[40,41] they are over 20–50 times larger than the typical boxes used for fully atomistic bulk glassy systems.[26,27,29] Further complications arose from the necessity to evaluate properly the nonbonded interactions in order to keep the simulations as realistic as possible. Although the polyimide matrices were prepared with full excluded-volume and electrostatic nonbonded interactions, calculations related to the diffusion had to be restricted to very small and highly mobile helium-like gas probes.[30,31] In the present work, the free-standing membrane has been reduced to a width of ∼60 Å, i.e., 49 800 atoms in 24 ODPA−ODA chains of 2075 atoms each. While this still remains a lot larger (by at least a factor 10) than what is currently used for fully atomistic simulations, it allows us to follow oxygen adsorption, penetration, and diffusion through the membrane over a total of 13 000 ps, thus making this study a lot more realistic than the former ones.[28,30,31] In addition, oxygen exhibits both a lower diffusion and a much higher solubility in polyimides than helium or other related small probes,[4] two features that could not be studied in our 141 100-atom membrane using currently available computational resources.

Although the preparation of the 49 800-atom membrane resembles that of the former one,[28,31] its computational details will be briefly summarized in section 2 along with the specific features related to the insertion of oxygen. Section 3.1 will describe the ODPA−ODA membrane and compare it to other works reported in the literature both on rubbery and glassy polymers.[28,30,31,39,42–59] Its permeation parameters with respect to O_2 will be characterized in section 3.2. There are only very few cases of fully atomistic membranes used to study gas transport in polymer matrices,[45,57] and with the exception of our polyimides,[28,30,31] we are not aware of any other work published on realistic glassy membranes with the electrostatic interactions switched on.

2. Computational Details

2.1. Model. The chemical structure of an ODPA−ODA polyimide chain is shown in Figure 1. Each chain has a total of 40 monomers and 2075 atoms. The force field and the

* To whom correspondence should be addressed. E-mail: sylvie.neyertz@univ-savoie.fr.

10.1021/ma7026676 CCC: $40.75
Published on Web 03/13/2008

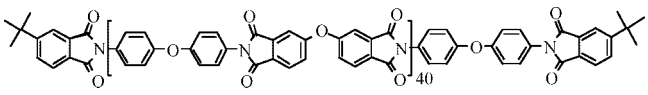

Figure 1. The (ODPA−ODA) polyimide chain.

parameters for the polyimide were the same as described before,[27–31,60] while the penetrant parameters were taken from the two-center Fisher−Lago potential for pure oxygen.[61] Bonds were kept rigid in order to be able to use an integration time step of 10^{-15} s, and "bonded" interactions arising from near-neighbor connections in the structure were described by angle-bending, torsional, and out-of-plane interactions. The "non-bonded" excluded-volume and electrostatic potentials were applied to all atom pairs separated by more than two bonds on the same molecule or belonging to different molecules. The chosen analytical form for the van der Waals interactions was the Lennard-Jones (LJ) 12–6 equation, with standard combination rules for all cross-terms.[18] It should be noted that the gas−gas interaction parameters were not artificially set to zero in order to keep the simulations as realistic as possible and in particular with regard to the buildup of an adsorbed layer at the polymer surface. Long-range electrostatic energies were evaluated using the Ewald summation method, both in the membrane and in the associated bulk models.[62,63]

All calculations were performed using the MD code of the *gmq* package[64] in its parallel form and *ddgmq*[65] on the French IDRIS (Orsay) and CINES (Montpellier) supercomputing centers as well as on local resources at the University of Savoie.

2.2. Preparation Procedure for the Free-Standing Membrane and the Bulk Models. The preparation procedure for fully atomistic polymer films is nontrivial, and to date, relatively few techniques have been described in the literature. By far the most common approach is that of extending the *z*-axis in order to eliminate interactions of the parent chains with their images in one direction.[44,46,50,55,56,59,66] However, this requires significant mobility of the polymer in order to relax from bulk to surface-like chains, which is virtually impossible in the case of rigid chains such as polyimides. In principle, it is also possible to use reverse mapping from equilibrated coarse-grained models using either Monte Carlo (MC)[44,67,68] or MD[69–74] simulations. The main drawback with multiscale approaches is that they require well-parametrized coarse-grained models at the right temperature for the molecules under study, something which is beyond the scope of this work. It is not expected either to be straightforward for polyimides as the only known attempt on BPDA-based bulks led to surprisingly low model densities.[75] An intermediate approach, closer to our technique, is that which has been used to compress a bulk polyisoprene chain with a repulsive wall, by starting from a box big enough to contain a single chain under the periodic boundary conditions.[76,77]

Our basic idea for creating ODPA−ODA films (see refs 28, 30, and 31 for full details) was to mimick the experimental solvent-casting process, which involved preparing a 10% (w/w) solution of the polymer in *m*-cresol, casting it onto a clean glass plate, removing the solvent through an appropriate heat treatment, and finally peeling off the film from the glass plate.[5,40,41,78,79] 24 chains were generated independently using hybrid Pivot MC-MD single-chain sampling[28,80] and distributed in a 10% solution simulation box with a virtual density of a (90% *m*-cresol/10% ODPA−ODA) mixture. Only the *z*-direction was expanded while the basis vectors in the *x*- and *y*-directions were left at the value expected from the experimental ODPA−ODA density, since the surface area of a film remains quasi-constant throughout the experimental process. Following the progressive introduction of the full potential and local relaxation, a four-layer diamond-lattice impenetrable wall was subsequently added on either side of the "solvated" polymer. The process of densification resulting from solvent evaporation was modeled by compressing the wall + polymer system in the *z*-direction until bulk density was reached in its center. High-temperature constant-volume NVT runs were then carried out at 700 K to relax internal stresses and the membrane was subsequently cooled to 300 K at a rate of -1 K ps^{-1}. In all cases, the temperature was maintained through loose coupling to a heat bath[81] with a coupling constant equal to 0.1 ps. At that stage, the confined membrane had dimensions of $112 \times 113 \times 58$ Å^3 and was allowed to settle for 100 ps, the drift in Coulombic energy being less than 0.1% over the last 50 ps. The box size was subsequently expanded to $112 \times 113 \times 130$ Å^3 with the wall being pushed away to its boundary, in order to avoid any excluded-volume interactions with the polymer while preventing gas probes from escaping into the vacuum. Once free to move, the polymer chains relaxed slightly in the *z*-direction to give a membrane width of ∼60 Å. The Ewald sum was found to converge[62,63] using $\alpha = 0.15$ Å^{-1}, $K_{max} = 13$, and a real-space truncation of 10 Å. The van der Waals potentials were also truncated at 10 Å. This 49 800-atom free-standing membrane was run on its own for 500 ps at 300 K, prior to introduction of the gas. The drift in Coulombic energy was less than 0.2% over the last 50 ps, which was deemed as being very reasonable for a glassy nonequilibrium system.

Although this atomistic preparation procedure is rather intrincate, it is clear that it might still suffer from some shortcomings.[28,30,31] The first one is that it would be preferable to simulate a realistic solution with explicit solvent molecules. Indeed, it has been shown for coarse-grained bead−spring models that it is possible to dissolve the polymer in a solvent and subsequently evaporate the solvent using molecular simulation methods.[82,83] However, for realistic solvents and fully atomistic glassy polymers, this is simply impossible in terms of current computational resources. Another problem could be the influence of an ever-changing concentration on the conformational properties of the chains, which is unknown and difficult to incorporate a priori in any simulation given the very slow relaxation times. A third problem is that the combined effects of the relatively "small size" of the model (at least with respect to experimental dimensions), the preparation procedure, and the very low mobility led to chains being actually more surface-like than bulk-like. This shortcoming can be partially compensated by running separate bulk models. However, it will be shown in section 3 that the structural features of our free-standing membrane are in excellent agreement with published results on the surface-layer chains reported for much shorter, more flexible, and usually less-realistic polymers, in which the system sizes and relaxation times often allow for the gradual change from surface layers to bulk-like structure in the middle of the membrane models.[28,31,39,43,44,47,48,50,51,53,55–59,66,67,76,84–87] This indicates that our preparation technique gives at least reasonable configurations for the surface-layer chains of our polyimide.

In order to compensate for the lack of bulk-like structure in the middle of the membrane model, a 6225-atom ODPA−ODA bulk similar to that used previously[27] was run under NPT conditions; i.e., the on-diagonal and off-diagonal components of the pressure tensor **P** are maintained by loose coupling with a pressure relaxation time of 5 ps,[88] but the simulation box is allowed to relax toward its equilibrium shape and density. This "normal bulk" had a density of 1377 kg m^{-3}, i.e., within 0.7% of the experimental value of 1368 kg m^{-3}.[40] In addition, a lower density bulk was constructed by driving smoothly the "normal-density" bulk from an average side length of 41.4 to 41.8 Å. This second bulk model had a density of 1330 kg m^{-3}, similar to the middle of the membrane model, and will be referred to

afterward as the "97% density" bulk. It was relaxed for 500 ps under NVT conditions.

2.3. Oxygen Insertion. Gas insertion in the bulk models was carried out by superimposing both matrices with a pure oxygen simulation box of density 250 kg m^{-3} of the same size and shape and selecting those molecules which overlapped least with the polymer atoms. However, since the bulk simulation times allowed for the Einstein regime for diffusion to be attained, there was no dependence of the results on the initial positions of the penetrants. The number of oxygen molecules n_p to insert into the bulk models was set to 25, which has been shown to give sufficient statistics.[27] In addition, it should imply rather reasonable external pressures considering the solubility of oxygen. Indeed, for small penetrants that do not really swell the matrix, there is a fairly simple relationship[28,30,31] between the number of gas molecules in the polymer, n_p, the volume of the polymer, V_p, the temperature T, the Boltzmann constant k_B, and the probability of insertion of the gas into the polymer, p_{ip}:

$$P \approx \frac{n_p k_B T}{p_{ip} V_p} \tag{1}$$

p_{ip} is usually obtained from Widom's test-particle insertion method,[27,89,90] in which a virtual gas molecule is repeatedly inserted at random sites into the matrix and the changes in potential energy associated with the insertion, ΔU, are calculated. This technique can give a good approximation of the solubility, S, of relatively small penetrants in a polymer:[89,90]

$$S \approx p_{ip} = \left\langle \exp\left(-\frac{\Delta U}{k_B T}\right)\right\rangle \tag{2}$$

Within the framework of Henry's law, i.e., the solubility of the dissolved gas is linearly proportional to the pressure P, p_{ip} can be expressed as a solubility coefficient $S_c = p_{ip}T_{STP}/(TP_{STP})$, where T_{STP} and P_{STP} are the standard temperature and pressure (STP: 273.15 K; 1.013×10^5 Pa) and T is the temperature of the measurement. When the penetrant has a very low solubility, p_{ip} is well under 1, and the external pressure P corresponding to 25 penetrants in a typical MD size box can easily be of the order of several hundred bar, as was found with helium and related probes.[28] Penetrants with higher solubilities will correspond to much lower external pressures, but in these cases, eq 1 has to be used with caution as deviations from Henry's law may be significant; e.g., carbon dioxide[26] acts as a plasticizer in certain glassy polymers.[91,92] On the other hand, Widom's method is commonly used in polyimides for O_2 or N_2, where a factor of 2–5 is typically found between calculated solubilities and experimentally derived ones.[25,26,28] In the pure 6225-atom ODPA−ODA bulk, $\langle p_{ip}\rangle = 3.0$ over several million trial insertions, which corresponds to $\langle S_c\rangle = 2.7$ cm^3 (STP) cm^{-3} bar^{-1}. The large standard deviations of 1.8 on $\langle p_{ip}\rangle$ reflect the fact that oxygen solubility is very dependent on the local details of the structure, and indeed if the same analysis is carried out on a much larger 56 025-atom bulk,[27] we get a $\langle p_{ip}\rangle = 2.5$ with a standard deviation of 0.7, i.e., $\langle S_c\rangle = 2.2$ cm^3 (STP) cm^{-3} bar^{-1}. The latter is in better agreement with the experimental range for O_2 in polyimides[3,25,26,93–97] of the order of 0.5–2.0 cm^3 (STP) cm^{-3} bar^{-1}. This level of agreement is actually quite good as several factors are likely to affect these results: on the one hand, standard classical molecular models are still rather primitive with e.g. empirical potentials, combination rules,[29] and fixed point partial charges, while on the other hand, experimental solubilities are usually only obtained indirectly from the permeability and diffusion and are prone to large errors. Using eq 1, our $\langle p_{ip}\rangle$ implies that 25 oxygen molecules should correspond to an external pressure P of ~5 bar in our bulk model, which seems very reasonable.

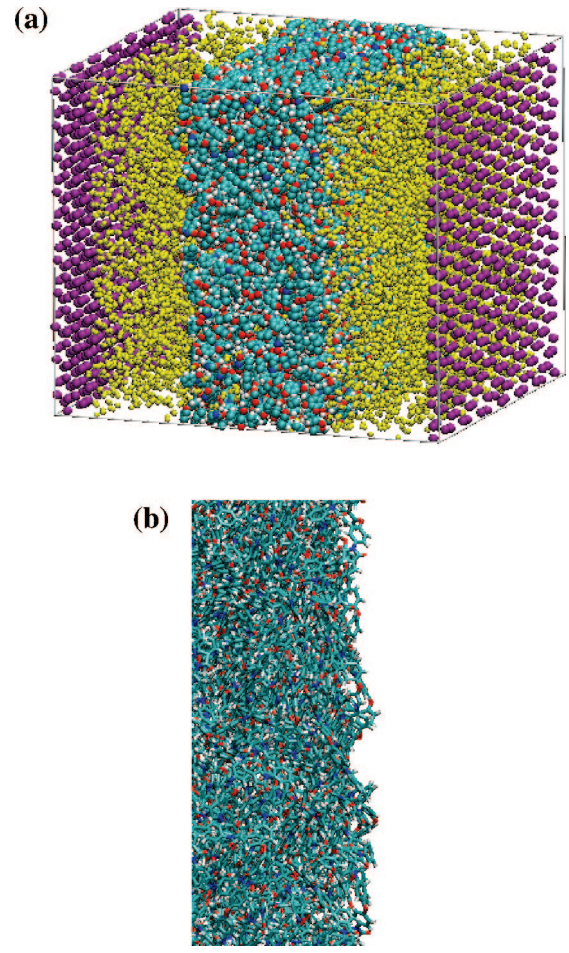

Figure 2. (a) Snapshot at 10 000 ps displaying the membrane, the O_2 penetrants, and the wall which prevents them from escaping into the vacuum. (b) Close-up of the right polyimide interface. The color code is the following: cyan = polyimide C, red = polyimide O, blue = polyimide N, white = polyimide H, yellow = penetrant O, purple = wall atom. These schematic representations are displayed using the VMD 1.8.2 software.[98]

In the case of the membrane model, we insert equal numbers of gas molecules into the empty spaces between the membrane and the impenetrable wall at the start of each simulation, thus allowing us to follow the natural adsorption and uptake processes in a fairly realistic way. Estimates of the total amount of gas to insert can again be made from the solubility but are slightly complicated here by two other factors: the quantity of gas adsorbed onto the membrane surfaces and the rate of diffusion of the gas into the membrane. The thickness of the adsorbed layer is not a priori easy to estimate, being more a result we hope to get out of the simulation, but it is known that the diffusion of O_2 in dense polyimides is rather slow in comparison to the time scale available to MD simulations.[4] The problem will be then to have enough oxygen molecules going into and diffusing through the membrane within the production run. Both of these factors militate thus in favor of higher estimates of the amount of gas to insert. In a first instance, 3500 O_2 molecules were placed on either side of the ODPA−ODA membrane in order to improve the chances of obtaining statistically meaningful results. A snapshot of the system including the polyimide membrane, the wall, and the penetrants is shown in Figure 2a and a close-up of the right polymer interface in Figure 2b.

Before presenting the results, some further remarks are necessary. It has been previously shown that introducing ideal-gas penetrants on one side or on both sides of a membrane model leads to very similar permeation curves.[57] While the O_2

molecules do interact in our model, the number of penetrants actually entering the central part remains relatively low, and thus we are not in a regime where $O_2 \cdots O_2$ interactions are likely to be significant. This is confirmed by the spatial resolution of the trial insertion probability, $\langle p_{ip}(z) \rangle$, for an O_2 probe molecule interacting just with the pre-existing penetrants in the system. This probability remains close to 1 within the membrane (see later). It would of course have been possible to set the $O_2 \cdots O_2$ interactions to zero, but this immediately results into an artifact where the adsorption layer at the interface takes on unphysical proportions.

Another question that arises is the evaluation of the actual gas pressure in the reservoirs. This is complicated by the roughness of the polyimide surfaces (see Figure 2b) and, as will be shown, the accumulation of O_2 at the polymer interface, albeit less significant than in the case where $O_2 \cdots O_2$ interactions are set to zero. Two approaches were used. First, the average reservoir gas density was measured in the part where the z-resolved insertion probability (taking into account all other atoms) for an oxygen molecule, $\langle p_{ip}(z) \rangle$, was approximately equal to one; i.e., the penetrant can be considered as being in an ideal gas phase. A constant-volume controlled-temperature (NVT) simulation of a pure 1000-molecule O_2 system with the corresponding density of $\sim$350 kg m^{-3} gave a pressure of $P \sim 270$ bar. A further series of NVT simulations of O_2 in the density range from 20 to 380 kg m^{-3} showed that all associated pressures, P, were very close to those obtained from $PV = nk_BT$. Above a density of 380 kg m^{-3}, they start deviating from the ideal gas approximation by more than 1%. A second approach used a direct measurement of the P_{zz} component of the pressure tensor from the atomic momentum flux[99] across virtual interfaces placed perpendicular to the z direction in the gas reservoirs. In the case of the model of oxygen used here, the momentum flux contains kinetic contributions from atoms that cross the interface plus the contributions of intramolecular (rigid bonds) and intermolecular forces. The average value of P_{zz} obtained was again $\sim$270 bar, thus confirming the indirect approach and the quasi-ideality of the gas in the center of the reservoirs.

As the reservoir pressures obtained were higher than those typically used in experimental conditions,[41] further simulations were performed to assess whether the pressure had any influence on the results. The membrane model was run from the start and for about 2500 ps with smaller 500-molecule reservoirs. In this case, the average O_2 density in the middle of the gas reservoirs was $\sim$33 kg m^{-3}, which corresponded to a pressure of $\sim$26 bar. However in 2500 ps, only 62 O_2 molecules per reservoir had entered the middle part of the membrane ($-13 < z < +13$ Å) vs 203 O_2 for the larger reservoir simulation. It is worth noting that the $203/62 \approx 3$ gas number ratio inside the membrane is quite different to the $3500/500 = 7$ ratio for the initial number of gas molecules in the reservoirs. As the ratio of the average gas pressure in the reservoir suggests, the gas density ratio in the middle of the reservoir, averaged over 2500 ps of simulation, is found to be actually equal to $\sim$10. This ratio progressively decreases to $\sim$2–3 in the low-density part of the membrane. This behavior is consistent with the observed formation of an adsorbed layer of penetrant at the interface that tends to reduce the gas pressure in the center of the reservoir and is proportionally more important, the fewer the number of O_2 molecules initially introduced.

Experimentally, the effect of pressure on transport parameters in polymer membranes is well documented[4] and is reported as having little influence on the permeability for low-sorbing gases such as O_2 or N_2. However, it is clear that there is a gap between typical experimental pressures and those that can be reasonably used in simulations if results of any statistical significance are to be obtained. Work currently in progress indicates though that the diffusion mode inside the membrane is not much affected by the number of gas molecules placed in the reservoir. Unfortunately, these investigations are limited by the fact that the simulations take a long time to complete ($\sim$1 year), and a compromise has to be made between the applied pressure and gathering sufficient statistics to characterize diffusion. In the present case, the initial insertion of 3500 O_2 molecules into each reservoir thus seems a sensible choice. So, unless stated otherwise, all the results presented here are for this model.

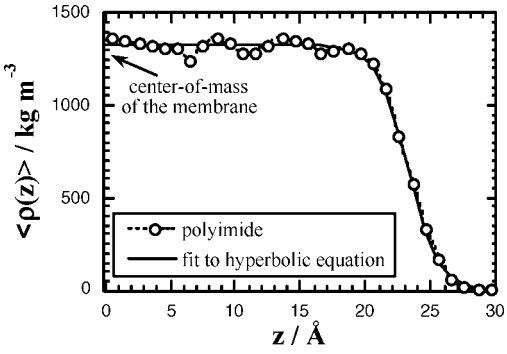

Figure 3. Symmetrized mass density distribution for the polyimide $\langle \rho(z) \rangle$ as a function of the distance z from the membrane COM (dashed line with circles). The slab width is 1 Å. The line is a nonlinear least-squares regression fit of $\langle \rho(z) \rangle$ to the hyperbolic equation given in eq 3.

Following equilibration, the "normal-density" + gas bulk model was run for 13 000 ps under NPT conditions while the "97% density" + gas bulk model was run for 5000 ps under NVT conditions, which allowed for their respective Einstein diffusion regimes to be attained. The production membrane + gas model was also simulated under NVT conditions for 13 000 ps. In all cases, configurations were stored at 10 ps intervals and thermodynamic and conformational data every 1 ps for postanalysis.

3. Results and Discussion

The main purpose of this work is to follow oxygen transport through our fully atomistic free-standing ODPA−ODA membrane and compare it to that in the corresponding bulks. Section 3.1 analyzes the structure and dynamics of the polymer membrane, while its permeation parameters with respect to O_2 are characterized in section 3.2.

3.1. Free-Standing Polyimide Membrane. This section reports the characteristics of the 49 800-atom free-standing polymer membrane. Most results displayed here and in the following sections will be symmetrized about the membrane center-of-mass (COM) so as to accumulate averages from both interfaces.

3.1.1. Densities and Interfacial Thickness. The slab mass density distribution as a function of the distance along the z-axis to the membrane COM, $\rho(z)$, is shown in Figure 3. As before,[28,31] the dense part of the model relaxes toward a slightly lower average value than ρ_{bulk} upon removal of the walls. This is linked to the flattening of the chain configurations, with local heterogeneities leading to fluctuations which can reach $\sim$65 kg m^{-3}. Those significant oscillations of $\rho(z)$ suggest an alignment of the chains with respect to the interface, but they are not sharp enough to really characterize separate layers. Unlike what has been reported in some rubbery polymers,[43,44,50,51,53,67] there is no evidence of specific species, e.g., chain ends, migrating to the surface in our glassy model. At the interface itself, the density profile is sigmoïdal, which is in agreement with other models of rubbery and glassy polymer free-standing surfaces.[28,31,39,43,44,47,48,50,51,53,55–59,66,67,76,84–87] On the other hand,

$\rho(x)$ and $\rho(y)$ remain very similar to ρ_{bulk}, since the membrane is held in place by the periodic boundary conditions along those two directions.

Defining a thickness for the interface and the "boundaries" of a free-standing membrane is rather subjective.[28,31] In addition, these parameters depend both on the property and on the way it is analyzed. For the mass density, it is common[47,48,52,55,59,84,85] to fit the sigmoïdal part of the density profile to the following hyperbolic equation[100,101]

$$\rho(z) = \rho_{middle} \frac{1 - \tanh[2(z-h)/w]}{2} \quad (3)$$

with ρ_{middle} being the density in the middle region of the film, h the location of the interface, and w the interfacial width. The fit of $\rho(z)$ averaged over the whole production run to the form of eq 3 is also displayed in Figure 3, and the resulting parameters are $\rho_{middle} = 1325$ kg m^{-3}, $h = 23.2$ Å for the location of the interface, and $w = 4.6$ Å for the interfacial width. Interestingly, the same w was found for the larger ODPA−ODA free-standing interface,[31] thus suggesting that the interfacial structural thickness is size-independent. This has also been seen in flexible poly(1,2-vinylbutadiene), although the bulk box edge lengths at the basis of both films considered were smaller, i.e., ∼24 and ∼30 Å.[56] ρ_{middle} is ∼3% lower than the experimental bulk value of 1368 kg m^{-3},[40] rather than the 5% found for the larger membrane. While this remains of the same order of magnitude, it is clearly dependent on the specific chain configurations in both models. In order to assess the effect of ρ_{middle} being inferior to ρ_{bulk}, the "97% density" bulk model was thus considered in addition to the "normal bulk". It should also be noted that some alternative ways to locate the interface are e.g. to define the midpoint where the density falls from its bulk-like value to its free surface value[58] or calculate $d\rho(z)/dz$ near the free surface.[47] The "midpoint" is located at $z = 23$ Å and the derivative reaches its minimum at $z = 22.5$ Å, which are almost identical to the hyperbolic equation approach.

Unlike larger penetrants such as carbon dioxide or small hydrocarbons,[4] O_2 is not expected to swell polyimide matrices. Indeed, the volume changes of the normal-bulk models (with or without penetrants) do not reveal any specific swelling effects that can be separated from the natural fluctuations of the glassy matrix. The membrane also slightly relaxes over its MD run with a tendency to marginally spread out. If $\rho(z)$ is subaveraged over 2 ns intervals and fitted to the form of eq 3, the location of the interface h increases at a rate of 0.04 Å ns^{-1}. Such variations are not unexpected in a nonequilibrium glassy film, but they do remain very limited and are subject to poor statistics. All properties will thus be averaged over the 100–13 000 ps interval of the production run, unless stated otherwise. In all cases, standard errors are smaller than the size of the symbols.

3.1.2. Chain Alignment and Flattening. Chain alignment can be characterized by second-order Legendre polynomial functions, $P_2(\cos\theta_\alpha)$, for specific atom triplets $\{i, j, k\}$ with θ_α being the angle between the α-axis and the vector between atoms i and k. They are defined as

$$P_2(\cos\theta_\alpha) = \frac{3}{2}\langle\cos^2\theta_\alpha\rangle - \frac{1}{2} \quad (4)$$

and their limiting values are −1/2 for a perfectly perpendicular alignment, 1 for a perfectly parallel alignment, and 0 for a random alignment of the vectors defining θ_α. These analyses were carried out for all mobile "pivot angles" of the polyimide chemical structure, i.e., the flexible C−O−C ether bridges of the ODA and ODPA moieties and the more rigid C−N−C ODA−ODPA linkages (see Figure 1).[60] Specific alignments were found neither in the three $P_2(\cos\theta_\alpha)$ of the bulk models nor in both $P_2(\cos\theta_x)$ and $P_2(\cos\theta_y)$ for the membrane. However, the $P_2(\cos\theta_z)$, which are given in Figure 4 for the C−N−C and the ODPA C−O−C pivot angles, tend toward −1/2 in the vicinity of the surface. This was noted before both for our polyimide membranes[28,30,31] and for many other polymer simulations.[32,33,37,38,43,44,48,50,51,58,59,66] Indeed, chains at the vicinity of an interface usually align in a parallel fashion with respect to the surface (i.e., in a perpendicular alignment with respect to its normal), albeit with various degrees of alignment. This feature is attenuated in a free-standing surface with respect to a confined surface (see e.g. the clear alignment of the polyimide aromatic rings in the $x-y$ plane at the vicinity of the wall in ref 30), and it decreases with increased roughness of the surface.[84] In addition, it depends on the flexibility of the chemical motive under consideration. However, it is clear from Figure 4 that this alignment persists into the core of the model, a similar feature found in our other polyimide membranes and obviously related both to the compression step and to the very low mobility of the glassy chains.[28,30,31] The flattening induced in the chains is confirmed by calculating the average chain radii of gyration $\langle S^2\rangle$ as a function of z as well as its component perpendicular to the interface, $\langle S_\perp^2\rangle$ (results not shown). Despite the limited statistics on the number of chains, the $\langle S_\perp^2\rangle$ represent at the most a negligible 1% of $\langle S^2\rangle$. This tendency of chains to be flattened at the proximity of a surface is also well-known[33–37,44,48,59,102] and has been called "pancakes" to describe their nearly two-dimensional behavior.[32–34,36,37,103]

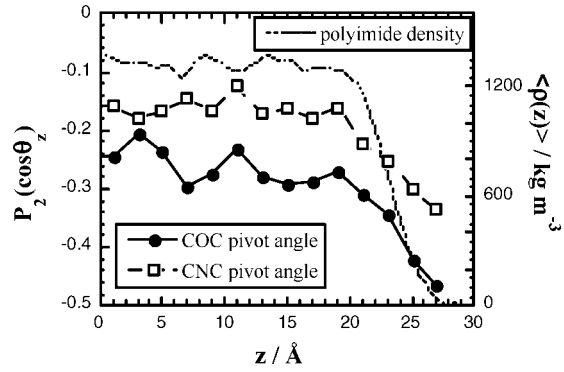

Figure 4. Left axis: symmetrized $P_2(\cos\theta_z)$ for different types of pivot angles as a function of the z distance from the angle middle atom to the membrane COM. The slab width is 2 Å. The COC angle displayed is the ODPA ether bridge, and the CNC angle is the ODPA−ODA link. Right axis: polyimide average mass density as a function of z.

It should be noted that, while the chains are both aligned and flattened, i.e., they can all be considered as characteristic of surface chains, the degree of order is certainly not reminiscent of layers, and the polyimide molecules are in reality intertwined.

3.1.3. Dynamics. It has been reported that the chain mean-square displacements over a given time interval t, $MSD = \langle(r_i(t + t_0) - r_i(t_0))^2\rangle$ with t_0 being a time origin, are enhanced in the vicinity of a free-standing interface,[47,49,53,86,87] even in the case of glassy matrices.[37,39,104] While the absolute values for the polyimide MSDs remain very small, Figure 5 shows that there is indeed the same increase in atomic mobility close to the interface that was noted before.[31] The MSDs only come back to the model core values over a distance of ∼15–20 Å from the gas reservoir and thus define a "dynamical interfacial thickness", which is larger than that obtained from the polymer mass density (see Figure 3). This dynamical thickness is indicated in Figure 5 and has been attributed to the transmission of mobility due to the molecular connectivity.[39] Interestingly, the fact that dynamical properties are affected on a larger range than structural properties has also been noted for other types of surfaces such as silica nanoparticles.[105] However, at the temperature under study, we cannot use specific concepts such as a fluidlike interfacial region, which interprets free-standing film behavior at the vicinity of the glass transition temperature.[51]

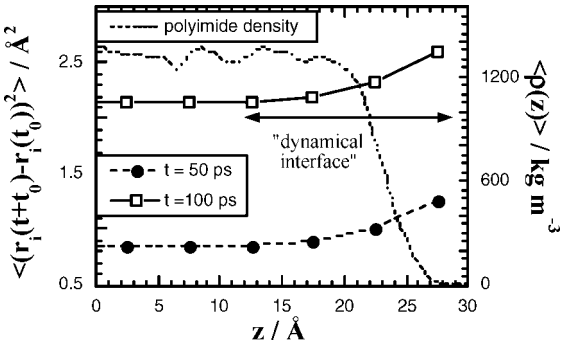

Figure 5. Left axis: symmetrized polyimide MSDs as a function of the z distance to the membrane COM for all atoms situated in a slab of width 5 Å at time t_0. Two time intervals are shown, i.e., $t = 50$ and 100 ps. The MSDs have been averaged over all polyimide atoms and all possible time origins of the production run. Right axis: polyimide average mass density as a function of z.

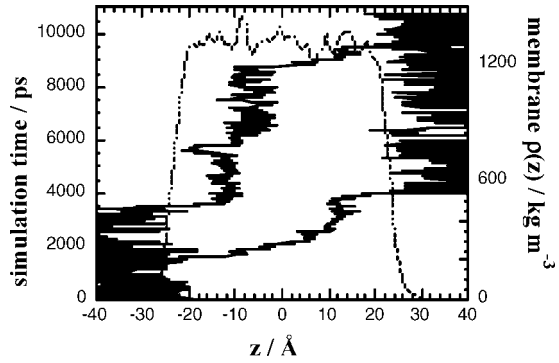

Figure 6. Trajectories along the z direction for two different oxygen molecules crossing the polyimide membrane (lines). The unsymmetrized average slab mass density for the polyimide (short dash) shows its actual position.

3.2. Oxygen Permeation. *3.2.1. Individual Trajectories.* Some trajectories for individual oxygen molecules which cross the membrane within the time scale of the 13 000 ps production run are displayed in Figure 6. The wide oscillations on each side of the membrane are characteristic of the gas reservoir and show that, despite a tendency for the penetrants to be adsorbed at the interface (see later), the O_2 molecules are still moving very much. On the other hand, their behavior in the dense part of the polymer is typical of small penetrants in glassy matrices; i.e., they oscillate within available free volumes and jump between different voids upon opening of temporary channels, with some jumps being productive and others unproductive in terms of diffusion.[28–31,90,106,107] O_2 is known to exhibit longer times of residence in the holes and less positional fluctuations than smaller probes such as He, but there are in reality as many possible paths as penetrants and a series of trajectories which are all different.

Note for example that in Figure 6 one of the oxygen molecules exhibits a fairly smooth trajectory while the other gets stuck for much longer until it finally finds a way to cross the membrane. In our former work, the z-component of the gas MSDs was found to be systematically lower than the x- and the y-components for small helium-like penetrants situated in the middle of the larger polyimide membrane, thus suggesting a degree of anisotropy in their transport.[28,30,31] In the present case, we do not see such an anisotropy as the x-, y-, and z-components of the MSDs of O_2 penetrants situated in the core of the membrane are of the same order of magnitude within the statistical resolution available. This behavior is likely to be related to the significant differences in nature between the probes used. The helium-like penetrants exhibit both a low solubility and a very fast diffusivity, which allow them to probe the entire available void space. On the other hand, the interactions between the soluble O_2 and the matrix are a lot stronger, and its motion is obviously more restricted by the local relaxations of the polymer.

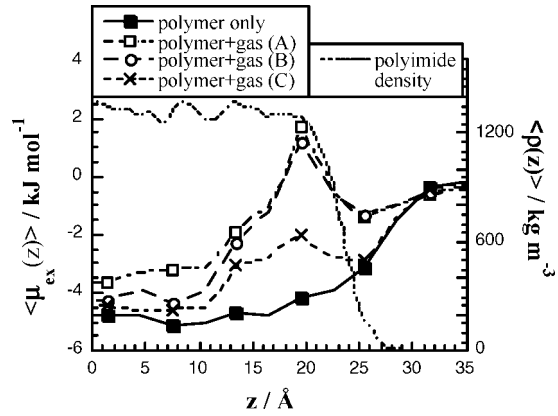

Figure 7. Left axis: symmetrized $\langle\mu_{ex}(z)\rangle$ for O_2 in the ODPA−ODA membrane as a function of z, with a histogram width of 3 Å. Insertion energies were calculated by taking into account either the polymer matrix on its own (black squares) or the polymer matrix and all other O_2 penetrants (white symbols and crosses). For the latter, (A) refers to data accumulated over the full 13 000 ps of the production run with the larger oxygen reservoir, (B) to the same case over the first 2000 ps, and (C) over 2000 ps for the smaller oxygen reservoir simulation. Right axis: polyimide average mass densities as a function of z.

3.2.2. Oxygen Solubility in the Free-Standing Membrane. The average probabilities of insertion of an O_2 probe into a polymer matrix obtained from Widom's insertion technique[89,90] $\langle p_{ip}\rangle$ (section 2.3) can be resolved as a function of z for a slab of given width $\langle p_{ip}(z)\rangle$. p_{ip} is also related to the excess chemical potential of the gas in the polymer, μ_{ex}, by

$$\mu_{ex} = -RT \ln\left\langle \exp\left(-\frac{\Delta U}{k_B T}\right)\right\rangle = -RT \ln(p_{ip}) \qquad (5)$$

which can then be resolved as a function of z. Results for $\langle\mu_{ex}(z)\rangle$ are presented in Figure 7 for 500 000 trials per configuration, a cutoff for van der Waals interactions equal to half the smallest box length (~56 Å), and a spatial z-resolution of 3 Å. The excess chemical potentials for O_2 in the pure free-standing membrane core (black squares in Figure 7) are clearly lower than $\langle\mu_{ex}\rangle = -2.3$ kJ mol^{-1} for the pure 56 025-atom bulk of similar size,[27] which means that solubility is enhanced in the membrane model. However, as was found earlier,[28,31] it can only partly be explained by the decrease in density: $\langle\mu_{ex}\rangle \approx -3.5$ kJ mol^{-1} for the pure 97% density bulk, while the membrane has a similar core density, albeit with aligned and flattened chains. The specific configurations associated with surface chains thus tend to favor solubility (or chemical potential) for O_2. Interestingly, the sigmoidal drop in polymer density at the structural interface does not lead to larger solubilities with respect to the model core. It is well-known that the relationship between densities and solubilities is far from being straightforward:[108] higher polymer density should lead to less space available for penetrants, i.e., lower solubility, but it should also lead to higher cohesive energy density, i.e., more solubility, which seems to be the dominant effect here. Insertions in the core are more favorable as O_2 is surrounded by the attractive polymer matrix, while those in the interfacial region only interact with the polymer on one side. Such a gradient in solubility can be a driving force for diffusion,[109,110] and indeed, there is an initial rapid adsorption of the penetrants onto the interface at the very start of the simulations (see section 3.2.3). In the gas reservoirs to either side of the membrane, the excess chemical potential eventually tends toward zero as expected.

The $\langle \mu_{ex}(z) \rangle$ were also calculated with the other gas penetrants in the system being taken into account in addition to the polymer. The unfilled squares and circles in Figure 7 refer to data accumulated for the larger O_2 reservoir system over the full 13 000 ps of the production run ("A") or over its first 2000 ps ("B"), respectively. The crosses come from the additional calculation with the smaller O_2 reservoir and are also accumulated over 2000 ps ("C"). In all three cases, $\langle \mu_{ex}(z) \rangle$ displays a peak around ~20 Å from the COM, which corresponds to a dip in the solubility at the start of the denser part of the matrix. Since "A" and "B" are almost superimposable in this region, it is likely to be related to the initial adsorption of the penetrants that leads to most of the voids in this region being quickly occupied by other oxygens. This stage is followed by a subsequent slower and limiting diffusion mode, whose boundaries lie at ~20 Å (see section 3.2.3). The slower filling up can indeed be seen in Figure 7 as one gets closer to the membrane COM. From "B" and "C" in Figure 7, the magnitude of the initial adsorption clearly depends on the external gas pressure, but we would need simulations with several different external gas pressures to better characterize this phenomenon. As stated above, work is currently in progress on this point and the first indications are that, unlike the initial adsorption phase, the diffusion coefficients of the limiting mode are not much affected by external pressure. The $\langle \mu_{ex}(z) \rangle$ were also calculated while excluding the interactions with the polymer from the analyses (not displayed) but retaining those with the gas. These gas−gas $\langle \mu_{ex}(z) \rangle \approx 0$ within the dense part of the membrane, which further justifies the introduction of the gas on both sides of the model in order to improve the statistics.

All these curves were averaged on time intervals where O_2 probes are continuously entering and moving slowly through the membrane. The overall picture that emerges is that the specific conformations of the polyimide membrane are indeed associated with a chemical potential gradient that attracts the penetrants to the surface. However, the incoming gas modifies the chemical potential profile so much that a peak is formed which acts as a barrier to further adsorption. Within the dense part of the membrane the chemical potential is also gradually modified by the relatively slow diffusion of the gas molecules into it. Ultimately, the chemical potential should eventually settle to a value characteristic of its core.

3.2.3. Diffusion Coefficients. Gas diffusion coefficients in the bulk models were obtained by averaging the gas MSDs over all penetrants and over all possible time origins of the production runs, t_0. In molecular dynamics simulations, the self-diffusion coefficient $D_{gas} = D_{bulk}$ is easily obtained from Einstein's equation providing that the crossover from anomalous to Fickian diffusion has occurred.[111,112] This condition can be identified by the fact that the slope of log(MSD) vs log(t) goes to one, which required ~8 ns for our normal-density bulk. The resulting O_2 diffusion coefficients are $D_{bulk} = 2.4 \times 10^{-7}$ cm^2 s^{-1} for the normal-density bulk and $D_{bulk} = 11.0 \times 10^{-7}$ cm^2 s^{-1} for the 97% density bulk. The applicability of Einstein's equation for self-diffusion as an estimation of the true diffusivity[113,114] in these glassy matrices was checked by running a separate bulk simulation with only five O_2 molecules. D_{bulk} was found to be roughly equal to 3.5×10^{-7} cm^2 s^{-1}, i.e., very close to the 25-molecule value. This is about 400 times slower than that of our He-like probe in our former model.[31]

The corresponding diffusion coefficient for O_2 in our glassy membrane, $D_{gas} = D_{membrane}$, cannot be obtained without a clear definition of the width of the membrane L. This is far from being straightforward since several possible definitions for the membrane thickness are possible (see section 3.1), and both membrane surfaces are highly heterogeneous (see Figure 2). Analyses were thus carried out using either $L = 46$ Å, which comes from eq 3, either $L = 36$ Å, which corresponds to the start of the dense part of the membrane, or $L = 26$ Å, which is situated both at the inner limit of the dynamical interface and in the part where the oxygen excess chemical potential tends to level off (Figure 7). The uptake curves, accumulated over both interfaces, are shown in Figure 8 as a function of the square root of time, $t^{1/2}$. When L is defined with respect to the mass density, i.e., $L = 46$ Å or $L = 36$ Å, the uptake curve first displays a jump characteristic of a rapid adsorption phase at very short times ($t < 250$ ps and for most of it $t < 10$ ps), which progressively changes into a slower rate of uptake and a more linear dependence with respect to $t^{1/2}$. The latter is also found with the much lower value of $L = 26$ Å, whereas the initial adsorption phase is now excluded. The densities, excess chemical potential, and uptake curves show that the penetrants mostly adsorb at the structural interface, since this phenomenon is already quite attenuated at $L = 36$ Å. However, O_2 is able to penetrate extremely fast into the membrane up to the dynamical interface, including through regions where the matrix is as dense as the core of the model, albeit with the solubility still increasing. As noted before, this behavior has to be compared to the fact that a gradient in chemical potential is also a driving force for mass transfer.[115] After the initial adsorption phase has ended, O_2 diffusion into the membrane can be uniquely described by the same limiting slope in all the uptake curves. This is best visualized in Figure 8 with the net uptake curve obtained with $L = 46$ Å but starting from 250 ps. Such a linear relationship between the weight gain of the polymer and $t^{1/2}$ is often taken as an indication that the system adopts Fickian diffusion.[114,116] However, the same curves also show a quasi-linear dependence as a function of t as well as a function of t^n with $^1/_2 < n < 1$ (results not displayed), which suggests that additional analyses are needed in order to characterize the actual diffusion regime. Nevertheless, the uptake curves vs $t^{1/2}$ displayed in Figure 8 are very useful to discriminate the initial adsorption phase from the rest of the diffusive behavior. Interestingly, the simulation where only 500 O_2 molecules were inserted into the reservoirs was found to qualitatively exhibit exactly the same behavior, although with less molecules entering the membrane core. The two-phase behavior thus seems to be present at both low and high gas pressures.

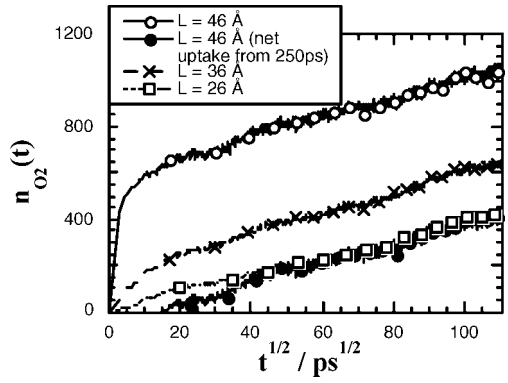

Figure 8. Number uptake of oxygen molecules by the membrane as a function of the square root of time. Because of the uncertainty in the definition of the membrane thickness, L, several values related to the interface have been considered.

The initial adsorption phase can be characterized by the time evolution of the z-dependent oxygen mass density, $\rho(z)$. Figure 9a displays the average gas $\rho(z)$ at 0, 1, 2, 4, and 50 ps. It confirms that there is a significant entry of O_2 into the dense part of the membrane within less than 5 ps. A comparison of the $d\rho(z)/dz$ minima for the different curves give us a rough estimation for the rate of advancement as being ~3 Å ps^{-1} as a function of z in this region, while D_{gas} in the middle of the

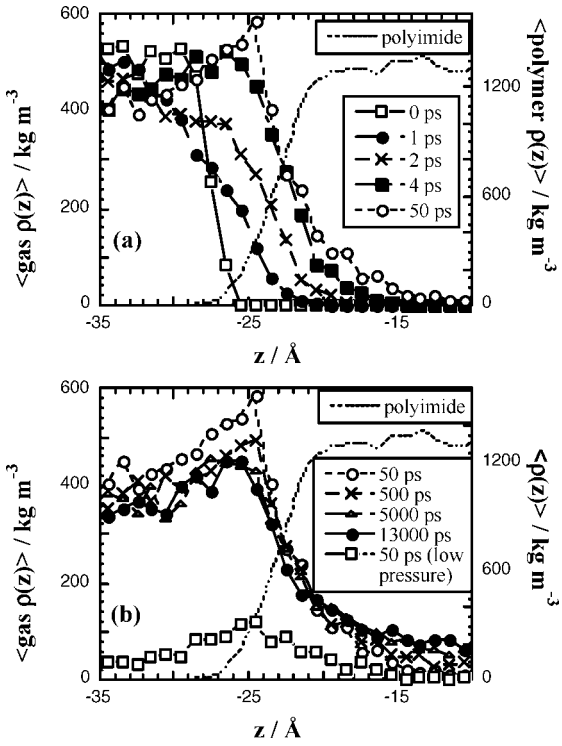

Figure 9. Left axis: time evolution of the average gas mass density distribution $\rho(z)$. Each curve corresponds to one single configuration. (a) covers the 50 ps interval at the start of the run while (b) describes the much longer 13 000 ps interval. Also shown in (b) is the gas density at 50 ps for the lower pressure run. Right axis: polyimide average mass density as a function of z.

enclosed gas reservoir can be estimated at ~25 Å^2 ps^{-1}. Mobility in the adsorption phase is thus certainly a lot closer to that of the pure gas phase than to the bulk. Once this phase is accomplished, the gas reservoir then settles at longer times (Figure 9b) into a profile which remains fairly stable throughout the 13 000 ps simulation. The time corresponding to the highest peak, $t = 50$ ps, seems to be the turning point between the very fast adsorption phase and the much slower uptake. The lower pressure system exhibits exactly the same phenomenon, but with a lower overall mass density. The ratio between both peaks at 50 ps is 5, i.e., lower than the 7:1 proportion of oxygens molecules in both types of reservoir, and eventually tends to a value of ~2–3 inside the membrane. The pressure effect is thus very much attenuated when the slow-uptake phase begins in the polymer core.

The slower diffusion modes were characterized as before[28,30,31] by fitting the gas time-dependent density distributions in the membrane of width L to the following solution of the one-dimensional diffusion equation in a semi-infinite system:[114,116]

$$c(z', t) = c_0 \,\mathrm{erfc}\left(\frac{z'}{\sqrt{4D_{\mathrm{gas}}t}}\right) \tag{6}$$

In eq 6, c is the penetrant concentration, D_{gas} is its diffusion coefficient, t is the time interval, and z' is the coordinate in a reference system where $z' = 0$ is the left edge of a medium which extends to $z' = +\infty$. z' is thus related to z by $z' = z + L/2$. The following boundary conditions are also required: $c(z' \geq 0, t = 0) = 0$; $c(z' = 0, t > 0) = c_0$. In the case of a finite-length membrane of length L, this solution can only be used up until the penetrants start to exit from the far side of the membrane. However, the number of oxygens actually crossing the membrane on the simulation time scale remained so small (<0.2% for $L = 46$ Å) that this limitation could be safely

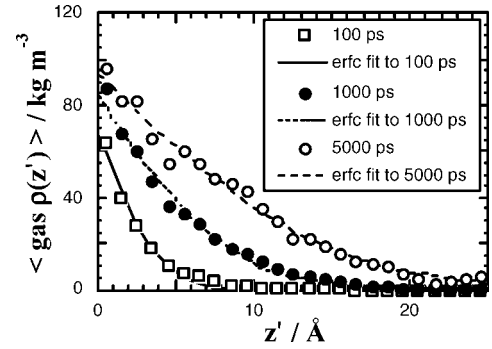

Figure 10. Mass density distributions of labeled oxygens as a function of their position in the membrane of width $L = 36$ Å at time intervals of 100, 1000, and 5000 ps. The actual profiles have been symmetrized, averaged over all possible time origins, and displayed with symbols. They are shown as a function of $z' = z + (L/2)$, and the slab width is 1 Å. The lines are fits to the erfc form of eq 6.

neglected here. Oxygen concentration vs time curves were obtained by artificially labeling gas probes as being on the "left", $z_i(t_0) < -L/2$, or on the "right", $z_i(t_0) > L/2$, at any particular time origin t_0 and then subsequently following the evolution of the distributions of these t_0-labeled atoms. All possible time origins were used, and the distributions for "left" and "right" molecules were subsequently symmetrized. The actual curves obtained for $L = 36$ Å are displayed as a function of z' with symbols only in Figure 10 for time intervals of 100, 1000, and 5000 ps. The lines are best fits to the erfc form given in eq 6 with c_0 and D_{gas} being treated as free parameters. It is clear that the form of eq 6 provides a reasonably satisfactory description of the gas density profiles. Equation 6 was thus systematically used to fit the t_0-tagged oxygen density distributions for many possible time origins and for different definitions of the membrane width, L. The best-fit values of both parameters obtained for different time intervals, $c_0(t)$ and $D_{\mathrm{gas}}(t)$, are given in parts a and b of Figure 11, respectively. For comparison, the time-interval-dependent gas diffusion coefficients in the bulk polyimide model, $D_{\mathrm{bulk}}(t)$, as obtained by simply dividing the corresponding gas MSDs at time t by $6t$ (and whose limiting values at long t are the quoted values for D_{bulk}) are displayed in Figure 11c. Note that the scales of Figure 11b,c are identical.

When short time intervals are considered, the gas concentration at the boundary $c_0(t)$ and the gas diffusion coefficient $D_{\mathrm{gas}}(t)$ vary rather much in a way which is dependent on L. Both these effects tend to disappear at larger time intervals. For definitions which set the membrane boundaries within its dense part, i.e., $L = 26$ Å to $L = 40$ Å, $c_0(t)$ increases progressively with time, which is consistent with a nonequilibrium uptake phase. On the other hand, larger L values, i.e., $L = 42$ Å and $L = 46$ Å which are situated respectively at the end and in the middle of the polymer low-density interface, display a decreasing $c_0(t)$ representative of a limited draining of the reservoir. An initial marked increase in c_0, characteristic of the fast uptake at the interface is still present at very short times, but the draining effect rapidly takes over. This further justifies the choice of a large reservoir in these kinds of simulations if one wants to take into account the fact that the external pressure remains quasi-constant in the experimental process. From Figure 11a, the value of $L = 40$ Å can be estimated as being the "true width" for the slow diffusion mode, i.e., that part of the membrane where the polymer density and c_0 become quasi-constant.

The behavior of $D_{\mathrm{gas}}(t)$ in Figure 11b is reminiscent of that of the bulk diffusion coefficient displayed in Figure 11c, which decrease as a function of t in the anomalous regime before settling to a limiting value D_{bulk} in the Einstein regime.[27] This is exactly what happens here for the membrane, with the larger

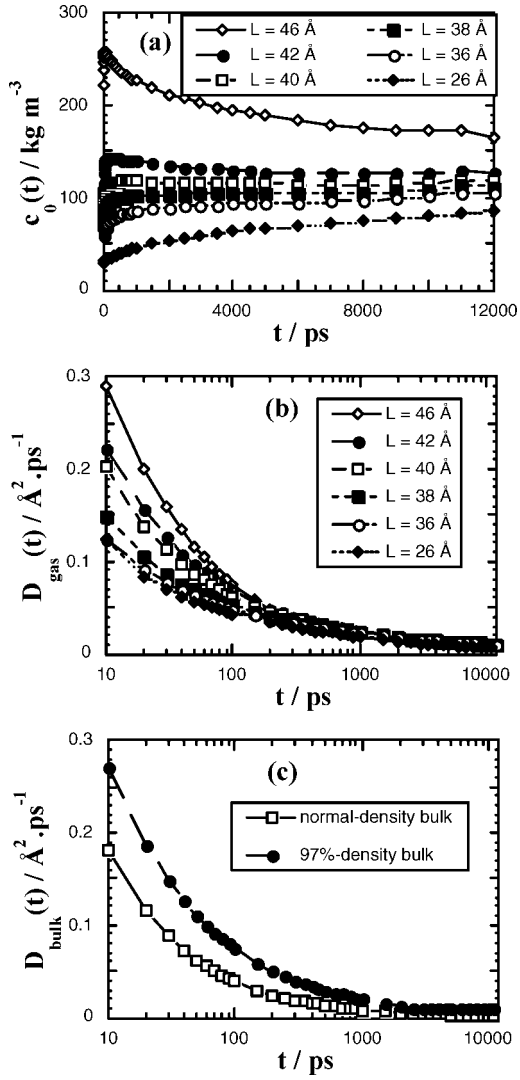

Figure 11. Time-interval t-dependence of the (a) c_0 and (b) D_{gas} parameters used in the erfc fits (eq 6) for the mass density distributions of t_0-tagged oxygens having entered the membrane of width L. (c) t dependence of the gas diffusion coefficients in the bulk polyimide models, $D_{bulk}(t)$, as obtained from the actual MSDs in the manner described in the text.

L values leading to faster $D_{gas}(t)$ at low time intervals because of the heterogeneities in the surface region. It has been suggested that anomalous diffusion systematically occurs in concentration-dependent diffusive processes, and this has been proven experimentally with diffusion experiments of high-concentration aqueous $CuSO_4$ into deionized water.[117] Interestingly, this first arose from a series of computer simulations based on cellular automata.[118] However, we are not aware of any experimental data on glassy polymer membranes that can be related to our model. In any case, whatever the choice of L, Figure 11b shows that the diffusion coefficient tends toward a constant limiting value after ~10 000 ps of simulation, i.e., $D_{membrane} \approx 0.009$ Å ps^{-1} $= 9 \times 10^{-7}$ cm^2 s^{-1}. While the system with the smaller reservoir was only run for 2500 ps, its $D_{gas}(t)$ as a function of t curve with $L = 40$ Å is found to be almost superimposable at small time intervals (within the statistical uncertainties) with that of the larger reservoir simulation. This suggests once again that $D_{membrane}$ is either independent or very weakly dependent on the applied pressure for the two cases examined here.

The oxygen diffusion coefficient through our model ODPA−ODA film, $D_{membrane}$, is rather close to $D_{bulk} = 11.0 \times 10^{-7}$ cm^2 s^{-1}, which was found for the 97% density bulk. This is only slightly faster than $D_{bulk} = 2.5 \times 10^{-7}$ cm^2 s^{-1} for the normal-density bulk, and it corroborates the results obtained earlier with the small repulsive probe in the larger membrane,[28,31] where diffusion was found to be mostly governed by the density prevailing in the polymer matrix.

4. Conclusion

A realistic MD simulation of oxygen transport through a fully atomistic polyimide ODPA−ODA membrane with the excluded-volume and electrostatic interactions being properly evaluated has been successfully carried out. This required a much larger model for the glassy polyimide matrix than is usually found in the literature. The specific procedure, loosely based on the experimental solvent-casting process, used to create the initial configurations gives typical features of free-standing membrane surface chains in terms of density and alignment.

Oxygen penetrants inserted on either side of the membrane model were found to exhibit two distinct mobility modes. The first one is a very fast adsorption phase of the gas at the membrane interface, which happens very rapidly at the start of the simulation and is clearly driven by the strong solubility gradient in this region. This leads to a pronounced peak in the gas density which persists throughout the simulation. Despite the strong adsorption in the interfacial region, O_2 motion takes place at a rate close to that found in the pure gas phase, and gas molecules are constantly entering and leaving this region. The second stage takes over after ~50 ps and is a much slower and limiting diffusion mode with a boundary situated at the start of the denser part of the matrix. The adsorption phase depends on the external pressure, but a compromise had to be found between the applied pressure and enough statistics to characterize diffusion. This led in the present case to the choice of a 3500-molecule O_2 reservoir, which corresponded to a fairly high pressure ($P \sim 270$ bar) compared to experiment. In spite of the fact that the gas still behaves ideally under these conditions, a systematic study of the effect of the external pressure on oxygen transport in these models is currently under progress. Preliminary results with a 500-molecule O_2 reservoir ($P \sim 26$ bar) suggest that, unlike the effect at the interface, the pressure effect on the limiting diffusion mode is in fact rather limited.

Oxygen motion through the dense polymer is characteristic of that generally found for small penetrants in glassy matrices; i.e., the penetrants jump between different voids upon opening of temporary channels within the matrix. Diffusion in the slower mode could be characterized using erfc fits, although they required a predefinition of the membrane width, L, which is far from being obvious in the case of such rough surfaces. The diffusion coefficient was found to vary at short time intervals in a similar way than in the bulk, which was attributed to anomalous diffusion. It eventually became constant at longer time intervals irrespective of the choice of L and showed that oxygen motion in such polyimide surfaces is mostly governed by the density of the matrix. Since solubility is also larger than in the bulk, it is clear that such interfacial polyimide structures cannot provide a "sieving" or "limiting" effect for gas transport.

It is important to note that very heavy computational resources are required if electrostatic interactions have to be included in such fully atomistic models and that this limitation prevents us from getting anywhere close to steady state. We did attempt to use excluded-volume interactions only but the membrane lost at least 10% of its cohesion, and this was discarded in favor of the more realistic representation reported here. Another word of caution is the preparation procedure for large-scale glassy models, since their limited mobility does not allow for the rearrangement of surface chains upon a simple extension of one of the simulation box axes. The strength of our technique is that it is based on the experimental solvent-casting procedure,

but there are clearly some technical points that would need further examination, such as the inclusion of specific solvent molecules or the effect of the compression rate. However, such models do provide a good representation of surface chains and bring a wealth of information on the underlying structures and dynamics. It would thus be interesting to apply this approach to different probes, i.e., either to penetrants similar to O_2, which do not modify much the matrix,[4,119–122] or even to more soluble gases such as CO_2, which are thought to lubricate the chain motions.[91,92]

Acknowledgment. The IDRIS (Orsay, France) and CINES (Montpellier, France) supercomputing centres and the MUST Linux server at the University of Savoie are acknowledged for their generous provision of computer time.

References and Notes

(1) Ohya, H.; Kudryavtsev, V. V.; Semenova, S. I. *Polyimide Membranes—Applications, Fabrication and Properties*; Kodansha Ltd.: Tokyo, 1996.
(2) Paul, D. R.; Yampolskii, Y. P. *Polymeric Gas Separation Membranes*; CRC Press: Boca Raton, FL, 1994.
(3) *Polyimides: Fundamentals and Applications*; Marcel Dekker: New York, 1996.
(4) Yampolskii, Y.; Pinnau, I.; Freeman, B. D. *Materials Science of Membranes*; John Wiley & Sons Ltd.: Chichester, 2006.
(5) Pinel, E.; Barthe, M.-F.; De Baerdemaeker, J.; Mercier, R.; Neyertz, S.; Albérola, N. D.; Bas, C. *J. Polym. Sci., Part B: Polym. Phys.* **2003**, *41*, 2998.
(6) McHattie, J. S.; Koros, W. J.; Paul, D. R. *Polymer* **1991**, *32*, 2618.
(7) Chen, K. M.; Wang, T. H.; King, J. S. *J. Appl. Polym. Sci.* **1993**, *48*, 291.
(8) Pandey, P.; Chauhan, R. S. *Prog. Polym. Sci.* **2001**, *26*, 853.
(9) Joly, C.; Le Cerf, D.; Chappey, C.; Langevin, D.; Muller, G. *Sep. Purif. Technol.* **1999**, *16*, 47.
(10) Recio, R.; Palacio, L.; Pradanos, P.; Hernandez, A.; Lozano, A. E.; Marcos, A.; De la Campa, J. G.; De Abajo, J. *J. Membr. Sci.* **2007**, *293*, 22.
(11) O'Brien, K. C.; Koros, W. J.; Husk, G. R. *Polym. Eng. Sci.* **1987**, *27* (3), 211.
(12) Kawakami, H.; Mikawa, M.; Nagaoka, S. *J. Membr. Sci.* **1996**, *118*, 223.
(13) Mensitieri, G.; Del Nobile, M. A.; Monetta, T.; Nicodemo, L.; Bellucci, F. *J. Membr. Sci.* **1994**, *89*, 131.
(14) Shishatskii, A. M.; Yampolskii, Y. P.; Peinemann, K.-V. *J. Membr. Sci.* **1996**, *112*, 275.
(15) Pfromm, P. H.; Koros, W. J. *Polymer* **1995**, *36*, 2379.
(16) Huang, Y.; Paul, D. R. *Polymer* **2004**, *45*, 8377.
(17) Kim, J. H.; Koros, W. J.; Paul, D. R. *Polymer* **2006**, *47*, 3094.
(18) Allen, M. P.; Tildesley, D. J., *Computer Simulation of Liquids*; Clarendon Press: Oxford, England, 1987.
(19) Smit, E.; Mulder, M. H. V.; Smolders, C. A.; Karrenbeld, H.; Van Eerden, J.; Feil, D. *J. Membr. Sci.* **1992**, *73*, 247.
(20) Zhang, R.; Mattice, W. L. *J. Membr. Sci.* **1995**, *108*, 15.
(21) Hofmann, D.; Ulbrich, J.; Fritsch, D.; Paul, D. *Polymer* **1996**, *37*, 4773.
(22) Hofmann, D.; Fritz, L.; Ulbrich, J.; Paul, D. *Polymer* **1997**, *38*, 6145.
(23) Hofmann, D.; Fritz, L.; Ulbrich, J.; Paul, D. *Comput. Theor. Polym. Sci.* **2000**, *10*, 419.
(24) Hofmann, D.; Fritz, L.; Ulbrich, J.; Schepers, C.; Böhning, M. *Macromol. Theory Simul.* **2000**, *9*, 293.
(25) Heuchel, M.; Hofmann, D. *Desalination* **2002**, *144*, 67.
(26) Heuchel, M.; Hofmann, D.; Pullumbi, P. *Macromolecules* **2004**, *37*, 201.
(27) Neyertz, S.; Brown, D. *Macromolecules* **2004**, *37*, 10109.
(28) Neyertz, S. *Soft Mater.* **2007**, *4*, 15.
(29) Neyertz, S. *Macromol. Theory Simul.* **2007**, *16*, 513.
(30) Neyertz, S.; Douanne, A.; Brown, D. *Macromolecules* **2005**, *38*, 10286.
(31) Neyertz, S.; Douanne, A.; Brown, D. *J. Membr. Sci.* **2006**, *280*, 517.
(32) Ten Brinke, G.; Ausserre, D.; Hadziioannou, G. *J. Chem. Phys.* **1988**, *89*, 4374.
(33) Bitsanis, I.; Hadziioannou, G. *J. Chem. Phys.* **1990**, *92*, 3827.
(34) Vacatello, M. *Macromol. Theory Simul.* **2001**, *10*, 187.
(35) Kumar, S. K.; Vacatello, M.; Yoon, D. Y. *Macromolecules* **1990**, *23*, 2189.
(36) Vacatello, M. *Macromol. Theory Simul.* **2002**, *11*, 53.
(37) Mischler, C.; Baschnagel, J.; Binder, K. *Adv. Colloid Interface Sci.* **2001**, *94*, 197.
(38) Mansfield, K. F.; Theodorou, D. N. *Macromolecules* **1991**, *24*, 4295.
(39) Mansfield, K. F.; Theodorou, D. N. *Macromolecules* **1991**, *24*, 6283.
(40) Pinel, E. Ph.D. Thesis, University of Savoie, France, 2001.
(41) Bas, C.; Mercier, R.; Sanchez-Marcano, J.; Neyertz, S.; Albérola, N. D.; Pinel, E. *J. Polym. Sci., Part B: Polym. Phys.* **2005**, *43*, 2413.
(42) Madden, W. G. *J. Chem. Phys.* **1987**, *87* (2), 1405.
(43) Mansfield, K. F.; Theodorou, D. N. *Macromolecules* **1990**, *23*, 4430.
(44) Doruker, P.; Mattice, W. L. *Macromolecules* **1998**, *31*, 1418.
(45) Ito, M.; Matsumoto, M.; Doi, M. *Fluid Phase Equilib.* **1998**, *144*, 395.
(46) Natarajan, U.; Mattice, W. L. *J. Membr. Sci.* **1998**, *146*, 135.
(47) Jang, J. H.; Mattice, W. L. *Polymer* **1999**, *40*, 4685.
(48) Jang, J. H.; Ozisik, R.; Mattice, W. L. *Macromolecules* **2000**, *33*, 7663.
(49) Torres, J. A.; Nealey, P. F.; De Pablo, J. J. *Phys. Rev. Lett.* **2000**, *85*, 3221.
(50) Chang, J.; Han, J.; Yang, L.; Jaffe, R. L.; Yoon, D. Y. *J. Chem. Phys.* **2001**, *115*, 2831.
(51) Jain, T. S.; De Pablo, J. J. *Macromolecules* **2002**, *35*, 2167.
(52) Xu, G.; Mattice, W. L. *J. Chem. Phys.* **2002**, *116*, 2277.
(53) Xu, G.; Mattice, W. L. *J. Chem. Phys.* **2003**, *118*, 5241.
(54) Xu, G.; Lin, H.; Mattice, W. L. *J. Chem. Phys.* **2003**, *119*, 6736.
(55) Ayyagari, C.; Bedrov, D. *Polymer* **2004**, *45*, 4549.
(56) Ijantkar, A. S.; Natarajan, U. *Polymer* **2004**, *45*, 1373.
(57) Kikuchi, H.; Fukura, M. *KGK Kautschuk Gummi Kunststoffe* **2004**, *57*, 416.
(58) Baljon, A. R. C.; Van Weert, M. H. M.; Barber DeGraaff, R.; Khare, R. *Macromolecules* **2005**, *38*, 2391.
(59) Prathab, B.; Aminabhavi, T. M.; Parthasarathi, R.; Manikandan, P.; Subramanian, V. *Polymer* **2006**, *47*, 6914.
(60) Pinel, E.; Brown, D.; Bas, C.; Mercier, R.; Albérola, N. D.; Neyertz, S. *Macromolecules* **2002**, *35*, 10198.
(61) Fisher, J.; Lago, S. *J. Chem. Phys.* **1983**, *78*, 5750.
(62) Ewald, P. P. *Ann. Phys.* **1921**, *64*, 253.
(63) Smith, W. *Comput. Phys. Commun.* **1992**, *67*, 392.
(64) Brown, D. The gmq User Manual Version 3: available at http://www.lmops.univ-savoie.fr/brown/gmq.html, **1999**.
(65) Brown, D.; Minoux, H.; Maigret, B. *Comput. Phys. Commun.* **1997**, *103*, 170.
(66) Clancy, T. C.; Mattice, W. L. *Comput. Theor. Polym. Sci.* **1999**, *9*, 261.
(67) Clancy, T. C.; Jang, J. H.; Dhinojwala, A.; Mattice, W. L. *J. Phys. Chem. B* **2001**, *105*, 11493.
(68) Jang, J. H.; Mattice, W. L. *Polymer* **1999**, *40*, 1911.
(69) Eilhard, J.; Zirkel, A.; Tschöp, W.; Hahn, O.; Kremer, K.; Schärpf, O.; Richter, D.; Buchenau, U. *J. Chem. Phys.* **1999**, *110*, 1819.
(70) Queyroy, S. Ph.D. Thesis, University of Savoie, France, 2004.
(71) Queyroy, S.; Neyertz, S.; Brown, D.; Müller-Plathe, F. *Macromolecules* **2004**, *37*, 7338.
(72) Hess, B.; León, S.; Van der Vegt, N.; Kremer, K. *Soft Matter* **2006**, *2*, 409.
(73) Harmandaris, V. A.; Adhikari, N. P.; Van der Vegt, N. F. A.; Kremer, K. *Macromolecules* **2006**, *39*, 6708.
(74) Harmandaris, V. A.; Reith, D.; Van der Vegt, N. F.; Kremer, K. *Macromol. Chem. Phys.* **2007**, *208*, 2109.
(75) Clancy, T. C. *Polymer* **2004**, *45*, 7001.
(76) Kikuchi, H.; Kuwajima, S.; Fukuda, M. *J. Chem. Phys.* **2001**, *115*, 6258.
(77) Kikuchi, H.; Kuwajima, S.; Fukuda, M. *Chem. Phys. Lett.* **2002**, *358*, 466.
(78) Pinel, E.; Bas, C.; Neyertz, S.; Albérola, N. D.; Petiaud, R.; Mercier, R. *Polymer* **2002**, *43*, 1983.
(79) Pinel, E.; Mercier, R.; Sanchez-Marcano, J. G.; Neyertz, S.; Albérola, N. D.; Bas, C. *C. R. Chim.* **2003**, *6*, 493.
(80) Neyertz, S.; Brown, D. *J. Chem. Phys.* **2001**, *115*, 708.
(81) Berendsen, H. J. C.; Postma, J. P. M.; Van Gunsteren, W. F.; DiNola, A.; Haak, J. R. *J. Chem. Phys.* **1984**, *81*, 3684.
(82) Tsige, M.; Grest, G. S. *Macromolecules* **2004**, *37*, 4333.
(83) Tsige, M.; Mattsson, T. R.; Grest, G. S. *Macromolecules* **2004**, *37*, 9132.
(84) Doruker, P.; Mattice, W. L. *Macromol. Theory Simul.* **2001**, *10*, 363.
(85) Ochoa, J. G. D.; Binder, K.; Paul, W. *J. Phys.: Condens. Matter* **2006**, *18*, 2777.
(86) Peter, S.; Meyer, H.; Baschnagel, J. *J. Polym. Sci.: Part B: Polym. Phys.* **2006**, *44*, 2951.
(87) Morita, H.; Tanaka, K.; Kajiyama, T.; Nishi, T.; Doi, M. *Macromolecules* **2006**, *39*, 6233.
(88) Brown, D.; Clarke, J. H. R. *Comput. Phys. Commun.* **1991**, *62*, 360.
(89) Widom, B. *J. Chem. Phys.* **1963**, *39*, 2808.
(90) Müller-Plathe, F. *Acta Polym.* **1994**, *45*, 259.
(91) Lin, H.; Wagner, E. V.; Freeman, B. D.; Toy, L. G.; Gupta, R. P. *Science* **2006**, *311*, 639.
(92) Bos, A.; Pünt, I. G. M.; Wessling, M.; Strathmann, H. *J. Membr. Sci.* **1999**, *155*, 67.
(93) Tanaka, K.; Kita, H.; Okano, M.; Okamoto, K. I. *Polymer* **1992**, *33*, 585.

(94) Tanaka, K.; Osada, Y.; Kita, H.; Okamoto, K.-I. *J. Polym. Sci.: Part B: Polym. Physics* **1995**, *33*, 1907.
(95) Coleman, M. R.; Koros, W. J. *J. Membr. Sci.* **1990**, *50*, 285.
(96) Ayala, D.; Lozano, A. E.; De Abajo, J.; García-Perez, C.; De la Campa, J. G.; Peinemann, K.-V.; Freeman, B. D.; Prabhakar, R. *J. Membr. Sci.* **2003**, *215*, 61.
(97) Saiz, E.; Gonzalez, M. M. L.; Riande, E.; Guzman, J.; Compan, V. *Phys. Chem. Chem. Phys.* **2003**, *5*, 2862.
(98) Humphrey, W.; Dalke, A.; Schulten, K. *J. Mol. Graphics* **1996**, *14*, 33.
(99) Haile, J. M. *Molecular Dynamics Simulation: Elementary Methods*; Wiley: New York, 1992.
(100) Helfand, E.; Tagami, Y. *J. Chem. Phys.* **1972**, *56*, 3592.
(101) Helfand, E.; Tagami, Y. *J. Chem. Phys.* **1972**, *57*, 1812.
(102) Smith, K. A.; Vladkov, M.; Barrat, J.-L. *Macromolecules* **2005**, *38*, 571.
(103) Izumisawa, S.; Jhon, M. S. *J. Chem. Phys.* **2002**, *117*, 3972.
(104) Alcoutlabi, M.; McKenna, G. B. *J. Phys.: Condens. Matter* **2005**, *17*, R461.
(105) Barbier, D.; Brown, D.; Grillet, A.-C.; Neyertz, S. *Macromolecules* **2004**, *37*, 4695.
(106) Gusev, A. A.; Müller-Plathe, F.; van Gunsteren, W. F.; Suter, U. W. *Adv. Polym. Sci.* **1994**, *116*, 207.
(107) Gusev, A. A.; Suter, U. W.; Moll, D. J. *Macromolecules* **1995**, *28*, 2582.
(108) Van der Vegt, N. F. A.; Briels, W. J.; Wessling, M.; Strathmann, H. *J. Chem. Phys.* **1996**, *105*, 8849.
(109) Thompson, A. P.; Ford, D. M.; Heffelfinger, G. S. *J. Chem. Phys.* **1998**, *109*, 6406.
(110) Thompson, A. P.; Heffelfinger, G. S. *J. Chem. Phys.* **1999**, *110*, 10693.
(111) Gusev, A. A.; Arizzi, S.; Suter, U. W.; Moll, D. J. *J. Chem. Phys.* **1993**, *99*, 2221.
(112) Gusev, A. A.; Suter, U. W. *J. Chem. Phys.* **1993**, *99*, 2228.
(113) Tepper, H. L.; Briels, W. J. *J. Chem. Phys.* **2002**, *116*, 9464.
(114) Tsige, M.; Grest, G. S. *J. Chem. Phys.* **2004**, *120*, 2989.
(115) Krishna, R.; Wesselingh, J. A. *Chem. Eng. Sci.* **1997**, *52*, 861.
(116) Crank, J. C. *The Mathematics of Diffusion*, 2nd ed.; Oxford University Press: Oxford, 1979.
(117) Küntz, M.; Lavallée, P. *J. Phys. D: Appl. Phys.* **2004**, *37*, L5.
(118) Küntz, M.; Lavallée, P. *J. Phys. D: Appl. Phys.* **2003**, *36*, 1135.
(119) Yamamoto, H.; Mi, Y.; Stern, S. A.; St-Clair, A. K. *J. Polym. Sci., Part B: Polym. Phys.* **1990**, *28*, 2291.
(120) Jia, L.; Xu, J. *Polym. J.* **1991**, *23*, 417.
(121) Stern, S. A. *J. Membr. Sci.* **1994**, *94*, 1.
(122) Li, Y.; Ding, M.; Xu, J. *Macromol. Chem. Phys.* **1997**, *198*, 2769.

MA7026676